Fuel 227 (2018) 334–344

Contents lists available at ScienceDirect

Fuel

journal homepage: www.elsevier.com/locate/fuel

Full Length Article

One-dimensional modeling and simulation of injection processes of bioethanol-biodiesel and bioethanol-diesel fuel blends

Eloisa Torres-Jimenez[a], Rubén Dorado[a], Breda Kegl[b,*], Marko Kegl[b]

[a] Dep. Mechanical and Mining Engineering, University of Jaen, Campus las Lagunillas, 23071 Jaen, Spain
[b] Faculty of Mechanical Engineering, University of Maribor, Smetanova 17, SI-2000 Maribor, Slovenia

ARTICLE INFO

Keywords:
Biodiesel
Bioethanol
Injection system
Mathematical model
Experiment
Simulation

ABSTRACT

This paper presents the development of a complete simulation model for a mechanical in-line injection system feed with diesel, biodiesel, bioethanol fuel blends. The mathematical model is built by using the AVL Boost™ Hydsim software, while the required input data is carefully derived by making use of existing data as well as formulas and numerical procedures described in this work. This setup enables relatively efficient formulation and set-up of the mathematical model as well as consistent and reasonably accurate derivation of input data.

The derived model is used to simulate the injection processes of various bioethanol-biodiesel and bioethanol-diesel fuel blends. The simulation results are compared to experimental data obtained on a Friedman-Maier type 12H100_h test bed at ambient temperature and several operating regimes. The results show that the compared injection pressure and needle lift histories are generally in a good agreement with the experimental ones. Consequently, the simulation model presented is fast and accurate enough to be engaged in various numerical procedures, ranging from investigations of influences of bioethanol addition to injection system optimization.

1. Introduction

It is now widely accepted that the major driver of rising temperatures are anthropogenic greenhouse gas emissions (CO_2, CH_4, N_2O) which are largely related to the burning of fossil fuels [1]. Besides of this, the related pollution, e.g., caused by road transportation, affects adversely human health [2]. Because of these reasons, stringent anti-pollution laws are imposed by the governments, which forces researchers to develop more efficient engines with lower emission levels. In general, this challenge can be addressed in two ways: by improving the engine characteristics and by using biofuels that produce less net greenhouse gases.

As the engines are becoming ever better and more sophisticated, further improvements are increasingly difficult to achieve. In this context, numerical process simulation in combination with systematic numerical optimization procedures are increasingly becoming an absolute necessity. Of course, simulation results can only be as good as the underlying numerical models. So, model accuracy is a very important attribute, which is unfortunately closely related to computational efficiency. At this point, it must be noted that optimization procedures are typically iterative ones and high computational efficiency is needed in order to ensure acceptable optimization times. In this context, it is generally desirable that: (a) the underlying models are at least reasonably accurate, (b) the computation times are acceptable, and (c) the model is developed as quickly as possible by engaging existing numerical simulation software. This paper addresses the development of such a model for a mechanically controlled in-line fuel injection system (FIS) engaged in a diesel engine and fueled by renewable or partially renewable fuel blends.

When it comes to good engine performance, low fuel consumption, and low emissions, the FIS is one of the most important parts because it defines fuel injection characteristics; and fuel injection characteristics are the key to lower engine emissions and lower fuel consumption, while keeping other engine characteristics at an acceptable level. A mechanically controlled FIS is a rather sophisticated mechanical system consisting of deformable solid parts, either fixed or moving, and of a fluid, present in liquid and gaseous form. The understanding and implementation of the physical phenomena involved in its modeling is a rather sophisticated task. Despite of this, previous researches have managed to develop reasonably accurate and computationally efficient models of injection systems for diesel engines fueled by regular diesel fuel [3–5]. Often, these models were later modified to analyze the system behavior when fueled by biofuels [6,7]. Although a model development from scratch may have the advantage of enabling more insight and influence on the behavior of each computational component, other options may also have their benefits. Most of all, it might be of

* Corresponding author.
E-mail address: breda.kegl@um.si (B. Kegl).

https://doi.org/10.1016/j.fuel.2018.04.118
Received 12 January 2018; Received in revised form 27 February 2018; Accepted 24 April 2018
0016-2361/ © 2018 Elsevier Ltd. All rights reserved.

benefit to engage as much of existing commercial software as possible. This may shorten the development time considerably although the model development might still prove quite difficult. These difficulties are typically related to proper selection of available model components, adequate description of boundary conditions, and derivation of correct input data and input functions. Once such a model is defined, it is almost unavoidable to test it thoroughly by using experiments.

In this work, the FIS modeling was done by using the AVL Boost™ Hydsim software [8], which allows simulating the injection system of an internal combustion engine. This software is developed for the dynamic analysis of non-stationary hydraulic and hydro-mechanical systems. It is based on the theory of one-dimensional fluid flow and dynamics of multibody systems. Its main application area is the simulation of fuel injection.

Besides of the injection system type, fuel injection characteristics depend significantly on fuel properties [9,10]. This is especially true for mechanically controlled in-line injection systems since the fuel transport way is rather long and its geometry is quite sophisticated. Additionally, the fuel transport itself is plagued by reflected pressure waves and cavitation. Precise determination of fuel properties like viscosity or sound velocity is therefore of very high importance.

In contrast to usual mineral diesel, the properties of various biodiesels and their blends with bioethanol are not so good investigated and documented, although these fuels can be used in internal combustion engines. For example, biodiesel, which is made from vegetable oils, can substitute diesel fuel totally or partially in a compression ignition engine. Meanwhile, bioethanol, which is made from sugar, starch crops and cellulose, makes the same for spark ignition engines. In this work both, diesel and biodiesel fuels, blended with low concentrations of bioethanol are addressed. These blends can be used to run a diesel engine as well, although they come with their own advantages and disadvantages [11–13].

This paper presents the development of a complete simulation model, consisting of the underlying mathematical model and input data. The mathematical model for an in-line injection system is built by using a commercial software and presented in detail with all involved components. Furthermore, the input required for the computation, consisting of simple data and functions, is also carefully prepared and explained. The developed simulation model is validated by experimental data obtained for neat diesel fuel, neat biodiesel made from rapeseed oil, and blends of 15% (v/v) bioethanol in diesel fuel and in biodiesel. The experimental parameters used to validate the simulation model are: needle lift history (h_n) and injection pressure history (p_{II}).

The structure of the paper is as follows. Section 2 presents the involved fuels and their properties. Section 3 describes briefly the experimental data acquisition system. In Section 4 the computational model with all involved components is described. Section 5 describes the preparation of needed input data and involved functions. In Section 6 the numerical results obtained by the proposed model are compared to the experimental one. Finally, the conclusions are summarized in Section 7.

2. Tested fuels and their properties

In the present study, injection characteristics are obtained and analysed for the following fuels: neat mineral diesel fuel without flow improver additives (D100), neat biodiesel from rapeseed oil (B100), a blend of 15% concentration by volume of bioethanol in biodiesel (E15B85) and a blend of 15% concentration by volume of bioethanol in diesel fuel (E15D85). In this paper, bioethanol is considered as an additive; for this reason, the concentration of bioethanol is set in no more than 15% by volume.

According to the manufacturer specifications, the tested bioethanol is produced from fermentation of sugars and satisfies the ISO 9001 specifications. The tested biodiesel is conforming to European standard EN14214; its purity is assured by its ester content being higher than the minimum value prescribed by the biodiesel standard. The tested diesel fuel is conforming to the standard EN590.

Table 1
Test injection system main specifications.

Fuel injection system characteristics	Direct injection system with wall distribution (M system)
Fuel injection pump type	Bosh PES 6A 95D 410 LS 2542
Main components	Plunger-in-barrel assembly, high-pressure (HP) tube, and injector
Pump plunger (diameter × lift)	9.5 mm × 8 mm
High pressure tube (HP tube) (length x diameter)	1024 mm × 1.8 mm
Injection nozzle (number × nozzle hole diameter)	1 × 0.68 mm
Needle opening pressure	175 bar
Maximal needle lift	0.3 mm
Start of delivery (static injection timing)	30 °CA BTC

In order to be able to simulate the injection characteristics, the physical and chemical properties of each fuel must be defined. Some of those properties of D100, B100, bioethanol-biodiesel blends, and bioethanol-diesel fuel blends, were obtained experimentally and published in previous work of the authors: the properties of pure diesel fuel and bioethanol-diesel fuel blends are described in [14], while pure biodiesel and bioethanol-biodiesel blends are addressed in [15]. The sound velocity of all involved fuels (at various pressures) was also determined in previous work; in most detail the results are given in [16,7] and the procedure is briefly presented in Section 3.

3. Experimental data acquisition

In order to validate the simulation model, first of all the experimentally obtained injection characteristics of neat biodiesel and diesel fuel, as well as E15B85, and E15D85 blends are needed. The corresponding tests were performed on a fuel injection system and test bed as specified in Table 1 and Table 2.

All details of the performed tests and the results are shown in a previous study [16]. It is worth, however, to describe briefly how the experiments were actually performed.

Fig. 1 shows the measured injection characteristics (p_I, p_{II}, and h_n histories) for (a) E15D85 at full load (FL) and pump speed of 1100 rpm, and (b) E15B85 at 75% load (75L) at 800 rpm pump speed. The maximum injection pressure is determined as the peak of the pressure p_{II}. Injection duration (time from needle opening to needle closing) and injection timing (start of fuel injection) are determined from needle lift history h_n. It should be noted that p_{II} does not correspond exactly to the actual injection pressure history. This is because p_{II} is not measured in front of the nozzle hole, but at the end of the HP tube, just before the injector inflow. The pressure wave needs some time to travel the distance between these locations and consequently the start of injection does not coincide with the 175 bar pressure (needle opening pressure) of p_{II}. Furthermore, the time of needle closing (h_n becomes zero) does not coincide with the needle closing pressure of p_{II}. In spite of these differences, p_{II} can be regarded as a relative good approximation of the injection pressure and the influence of fuel variation on the injection pressure is well reflected in the variation of the p_{II} history.

In addition to the injection histories, the sound velocity of all tested fuels was also obtained experimentally at various pressures up to 700 bars. These measurements were based on the principle of pressure wave propagation. Essentially, the testing device consists of a specified length of the high-pressure (HP) tube, two piezoelectric-based pressure transducers located at both ends of the tube, and a small plunger-type pump. The pump was used to induce a pressure wave, which was registered by both transducers and simultaneously acquired by an adequate measuring system [16,7]. The obtained results were fitted by a

Table 2
Test bed main specifications.

Test bed type: Friedman-Maier type 12H100_h Measured parameters	Description
Pressure at the beginning of HP tube (p_I)	Pressure transducer AVL 31DP 1200E, connected to the National Instrument module bridge amplifier SCXI-1520
Pressure at the end of HP tube (p_{II})	Piezoelectric transducer KISTLER 6227 with a charge amplifier Kistler
Needle lift (h_n)	Variable-inductance sensor (iron core placed within two inductance coils and attached to the injector needle) and an amplifier HBM KWS 3085
Pump speed (n)	Rotational pump speed
Fuelling (V_c)	Graduated test tube (mm^3/cycle). Injected fuel quantity is measured by collecting the injected fuel over 500 cycles.
% Load	Load (not by the fuelling but by the rack position)
Top Dead Center (TDC)	Optic sensor (a disk with a single cut-out attached to the pump shaft, and a light source with photo detector applied)
Computer aided measuring system	Description
Computer	Pentium III 600 MHz, 256 MB RAM
Multifunction card	AT MIO 16 E2
Signal conditioning	SCXI-1520
Application for data acquisition	Built in LabVIEW software. Used to control the operation of the multifunction card and for data logging and post processing

polynomial equation, which is used to estimate the bulk modulus of the fuel.

4. Mathematical model

The system under consideration is a mechanically controlled fuel injection system. It basically consists of a jerk pump, a constant pressure valve, a high-pressure (HP) tube, and an injector. This assembly was modeled by using the AVL Boost™ Hydsim software, where individual components of the assembly are tied together by engaging mechanical, hydraulic, or special connectors. Fig. 2 shows the actual final scheme of the assembly with all its main components, connections and boundary conditions.

The flow of the fuel through a single assembly to one cylinder can be simulated as a one-dimensional flow and the components can be considered rigid parts with the exception of special components like a spring. Based on these assumptions, the components of the FIS assembly were modeled as described in Table 3, where the needed boundary conditions are also given.

With appropriate input data, this model can be used to simulate injection characteristics of various fuels. It should be noted, however, that the usability and correctness of the model heavily depends on adequate input data that is typically not easily available.

5. Model input data

The input data needed for the mathematical model are related to fuel properties as well as to geometrical and mechanical parameters of the system. These data were mostly obtained either by measurements or from the literature. The remaining unknown parameters were estimated by adjusting the simulated injection pressure

5.1. Fuel properties

The basic input data related to fuel properties are summarized in Table 4.

The density ρ_0 at reference temperature and pressure for each blend (Table 4) was estimated by linear interpolation from the equations derived in [17,18] for diesel fuel density, biodiesel density, and ethanol density. These equations relate linearly the density ρ (kg/m^3) to pressure p (bar) and temperature T (°C). For other pressure/temperature conditions, AVL Boost™ Hydsim software was used to compute the density of the fluid by using the following exponential law:

$$\rho(p,T) = \rho_0 e^{\frac{1}{E}(p-p_0)-\alpha(T-T_0)}, \quad (1)$$

where α is the thermal expansion coefficient.

The bulk modulus of elasticity is given by (Eq. (2)) where the sound velocity was obtained by using the formulas derived experimentally, as described at the end of Section 3:

$$E = a^2\rho, \quad (2)$$

Neither kinematic viscosity ν nor surface tension σ were available experimentally for the studied blends. Therefore, these parameters were computed by linear interpolation (Eq. (3)) of neat fuel properties (diesel EN590, biodiesel and ethanol) obtained from AVL Boost™ Hydsim database as follows

$$\begin{aligned}\sigma_{blend} &= \psi_{Diesel}\sigma_{Diesel} + \psi_{Biodiesel}\sigma_{Biodiesel} + \psi_{Ethanol}\sigma_{Ethanol}\\ \upsilon_{blend} &= \psi_{Diesel}\upsilon_{Diesel} + \psi_{Biodiesel}\upsilon_{Biodiesel} + \psi_{Ethanol}\upsilon_{Ethanol}\end{aligned} \quad (3)$$

where $\psi_{neat\ fuel}$ is the concentration of the corresponding neat fuel.

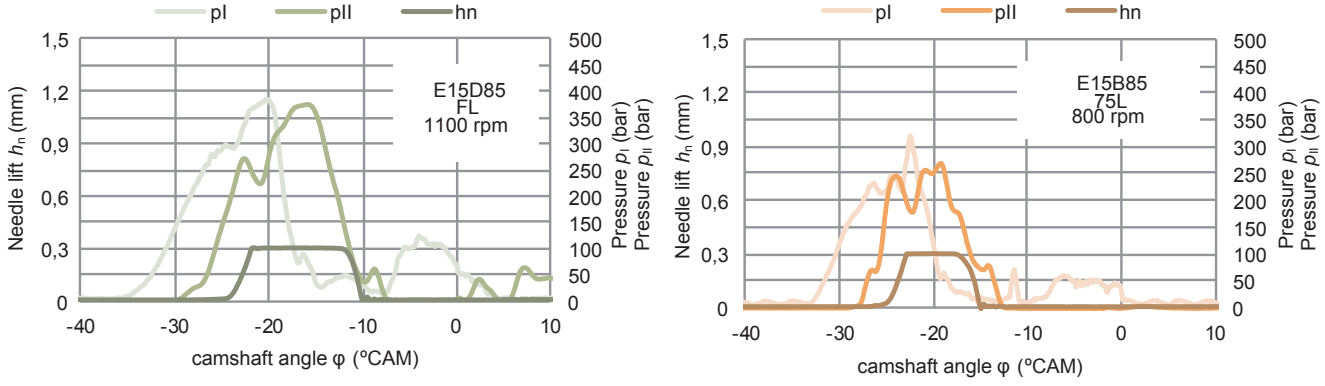

Fig. 1. Experimental pressures p_I and p_{II} and needle lift h_n histories for two random operating regimes and different fuels.

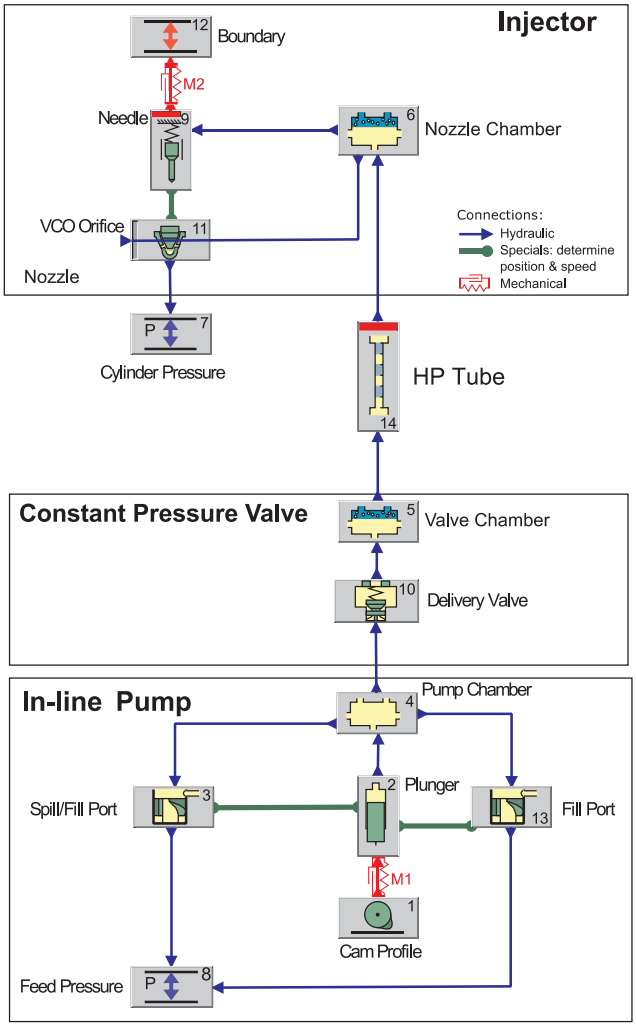

Fig. 2. General scheme of the FIS. Components, connections and boundaries implemented.

Table 4
Fuel properties at reference temperature (T_0) 293 K and reference pressure (p_0) 1 bar.

Fuel	Properties at T_0 and p_0			
	Density ρ_0 (kg/m^3)	Bulk Modulus E (N/mm^2)	Kinematic Viscosity υ (mm^2/s)	Surface Tension σ (N/m)
D100	834.50	1441.37	4.15	0.0262
E15D85	827.40	1387.75	3.75	0.0256
B100	880.05	1531.13	6.78	0.0330
E15B85	866.49	1472.95	5.99	0.0310

5.2. Mechanical, geometrical, and other parameters

The main mechanical, geometrical, and cavitation parameters of the injection system were either measured or estimated in order to adequately simulate each component shown in Fig. 2. Tables 5–7 summarize the measured parameters and parameters obtained by fitting the simulation to experimental data for: in-line pump, constant pressure valve + high pressure (HP) tube, and injector modules, respectively. Furthermore, we used the same value of vapour pressure (350 Pa) for all fuels under consideration because it turned out that its variation influenced the injection characteristics only negligibly. The AVL Boost™ Hydsim default values were assumed for most of the rest of the unknown parameters.

In order to take into account for the cavitation phenomena, AVL Boost™ Hydsim calculates the void fraction (gas fraction inside the fuel) according to the pressure. The cavitation model used is based on the Rayleigh-Plesset theory of bubble dynamics [19]. This setup requires to specify in advance the initial void fraction of fuel at some reference pressure. Note that this data is not readily available and has to be obtained somehow. In this work, the following procedure was used: the model was modified to run simulations for a sequence of consecutive initial void fraction values at 3 pump speeds (600, 800 and 1000 rpm). These simulation results were then used to find numerically the needed initial void fractions by minimizing the difference between experimental and simulated injection pressure. The same procedure was done for each tested fuel blend and a linear approximation was then used in order to define the needed initial void fractions at arbitrary pump speeds. Fig. 3 illustrates the results obtained for four fuels at 100% and

Table 3
Brief description of the mathematical model for each component of the FIS simulated. The number assigned to each component refers to Fig. 2.

FIS component	Number	Description of the model implemented
Cam profile	1	First order differential equations of motion. Mechanical boundary condition (external excitation)
Plunger	2	Motion of rigid element calculated by second Newton's law. One degree of freedom. Connected mechanically to the cam by a spring (mechanical connection M1).
Spill/Fill port	3	Flow equation through a gate valve in a straight tube. Bernoulli's equation. The program computes the flow resistance coefficient.
Fill port	13	
Pump chamber	4	Standard volume: Governing equation for isothermal flow (weakly compressible). Pressure time derivative is computed from the continuity equation.
Valve chamber	5	Two-phase volumes (fluid-gas mixtures):
Nozzle chamber	6	Governing equations for isothermal flow (weakly compressible). Pressure is computed from the continuity equation such as in standard volume but taking into account a two-phase flow. Cavitation: model based on Rayleigh-Plesset theory approximated model for the two-phase flow phenomenon.
Cylinder pressure	7	Pressure boundary condition.
Feed pressure	8	Pressure boundary condition.
Needle	9	One degree of freedom needle. Motion of rigid element calculated by second Newton's law (forces taken into account: hydraulic, mechanical, reaction, and shear from leakage forces). Connected mechanically to the boundary by a spring (mechanical connection M2).
Delivery valve	10	Motion of rigid element computed by second Newton's law (forces taken into account: hydraulic, mechanical (preload and damping forces of the valve spring), additional forces for input and output stops, and friction forces).
VCO orifice	11	Injected rate is computed from Bernoulli's equation. We use experimental data to define the effective cross-sectional flow area as a function of needle lift.
Boundary	12	Mechanical boundary condition.
HP tube	14	Second order fluid flow model based on the MacCormack finite difference algorithm. It is combined with flux corrected transport method. For two-phase flow, the bubble dynamic-cavitation model is applied.

Table 5
Mechanical, geometrical, and other parameters of the in-line pump module.

In-line pump	Number		
Cam Profile	1	Radius of cam base circle	12 mm
		Radius of roller	8.5 mm
		Follower acceleration at 1000 rpm	See Fig. 4a
		Young's modulus of cam material	206000 N/mm^2
		Effective roller contact width	11 mm
Plunger	2	Moving mass	0.12023 kg
		Plunger diameter (D_{pl})	9.5 mm
		Plunger spring preload	209.655 N
		Plunger spring stiffness	15380 N/m
Spill/Fill Port	3	Pre-stroke	1.87 mm
		Effective stroke (S_{eff})	$S_{eff}(mm) = \frac{4V_c}{\pi D_{pl}^2} + \frac{(\Delta p V_{pc})4}{\pi D_{pl}^2 E}$
			Δp = pressure rise during injection
		First helix angle	25°
		Plunger slot width	0.0023 m
		Narrowest area	5.75 mm^2
		Port diameter	0.0025 m
		Number of ports	1
Fill Port	13	Pre-stroke	0.00162 m
		First helix angle	25°
		Plunger slot width	0.0023 m
		Narrowest area	5.75 mm^2
		Port diameter	0.002 m
		Number of ports	1
Pump Chamber	4	Initial volume (V_{pc})	845.06 mm^3

Table 6
Mechanical, geometrical, and other parameters of the constant pressure valve + HP tube module.

Constant pressure valve and HP tube	Number		
Delivery Valve	10	Moving mass (body + 33% spring mass)	2.6884 g
		Maximum lift of valve body	4.3 mm
		Valve seat diameter	6 mm
		Retraction (unloading) volume	50 mm^3
		Opening pressure	20 bar
		Valve spring – Stiffness	15150 N/m
Valve Chamber	5	Initial Volume	836.6 mm^3
HP Tube	14	Line length (L)	1.0245 m
		Hydraulic diameter (d_t)	1.8 mm
		Fixed friction factor	0.02
		Adjusted from experimental data by fixing the variation between maximal p_I and maximal p_{II}	

75% load.

Note that the 3 tested pump speeds were chosen so that they cover the range of all characteristic engine speeds of the ESC (European Stationary Cycle) test for this particular engine. Based on this, one can assume that a linear interpolation can be used to calculate the initial void fractions at most practically interesting speeds. The loads (100% and 75%), however, were chosen as to provide data for the regimes considered in this paper. So, linear interpolation can probably be used only within some reasonable corresponding range.

Table 7
Mechanical, geometrical, and other parameters of the injector module.

Injector	Number		
Nozzle Chamber	6	Initial Volume	174.69 mm^3
		Temperature	80 °C (estimated)
Needle	9	Moving mass	0.0147566 kg
		Maximum lift of needle	0.0003 m
		Needle guide diameter	0.006 m
		Needle seat diameter	0.00303 m
		Squeezing fluid at needle closing – Damping coefficient (adjusted from experimental data fixing the slope of the needle closing curve)	100 Ns/m
		Needle seat/stop Stiffness (adjusted from experimental)	100000000 Nm
		Needle seat/stop damping (adjusted from experimental data fixing the vibration of the needle at maximal needle opening and at closing respectively)	500 Ns/m
VCO Orifice	11	Number of spray holes	1
		Diameter of one spray hole	0.68 mm
		Nozzle diameter at spray holes	1.54 mm
		Angle of needle seat	60.6°
		Effective cross-sectional flow area	See Fig. 4b
Nozzle Spring	M2	Preload force of the injector spring	372 N
		Stiffness	183800 N/m

According to Fig. 3, the initial void fraction at high pump speed and high load (100% and 75% load) is very low and practically independent of the fuel type. If pump speed decreases, the initial void fraction grows linearly with a slope that depends on the type of fuel and load. Adding low concentrations of ethanol (up to 15% v/v) to diesel fuel or to biodiesel does not modify significantly the initial void fraction. For a specific operating regime (different from high loads at maximum pump speed), the initial void fraction of diesel fuel is always higher than that of biodiesel. Lower loads tend to increase the initial void fraction slightly.

The described procedure for computing the initial void fraction combines numerical and experimental data. Theoretically, the experimental work could be avoided by using an adequate numerical procedure, for example, by changing the initial conditions (vapour volume, pressure, …) and running sequentially simulations until the initial conditions match with the final ones at the end of injection. Such procedures, however, typically tend to exhibit poor numerical stability and might be quite problematic.

6. Experimental validation of the model

AVL software estimates many parameters for each injection system component, for example, for nozzle elements it provides various output parameters related to: flow rate, cumulative flow, effective cross-sectional nozzle flow area, spray characteristics, injection power, injection duration, cavitation, etc. In order to verify the mathematical model, the numerically obtained injection characteristics have been compared to the experimental data given by our equipment. To simplify this comparison, the calculated response was used to compute the injection pressure p_{II}, corresponding to the pressure at the end of the HP tube (see Fig. 5), and the needle lift histories h_n. This simulation was performed taking into account the positions of both pressure sensors in the HP tube. The comparison has been done for each tested fuel at the following operating regimes: full load (FL) and 75% partial load (75L) for various pump speed regimes (1100, 800 and 600 rpm). Fuel temperature was 20 °C and the pump injection timing (angle of the start of fuel

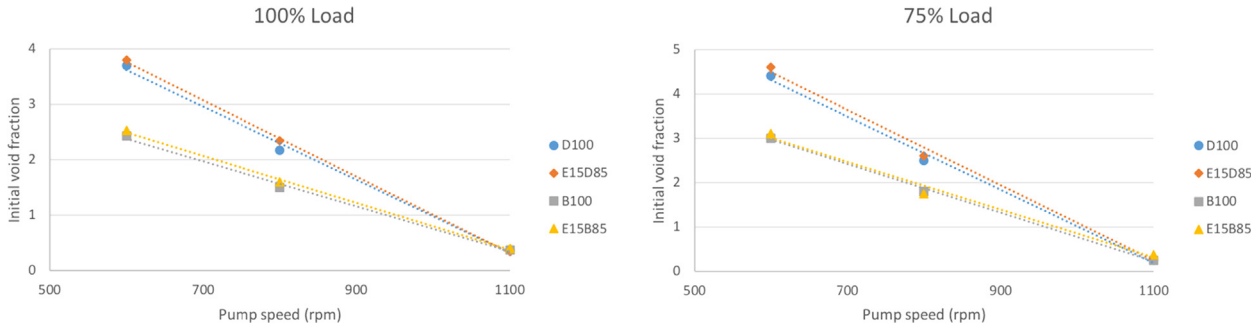

Fig. 3. Required initial void fractions (four fuels, 100% and 75% load) obtained by minimizing the difference between simulated and experimental injection pressure.

delivery) was 30 degrees of crankshaft angle before top dead centre (°CA BTDC).

Figs. 6–9 in the following depict the comparisons between experimental and simulated p_{II} and h_n for various fuels and loads at fuel temperature of 20 °C. At full load (FL), D100 and E15D85 are shown in Fig. 6 meanwhile B100 and E15B75 are shown in Fig. 7. At 75% partial load (L75), D100 and E15D85 are shown in Fig. 8 meanwhile B100 and E15B75 are shown in Fig. 9. The computation time for one operating regime was less than 10 s on a laptop with a 2.10 GHz Intel Core i7 CPU.

The injection pressure and needle lift histories presented in Figs. 6–9 show that the numerical simulation is in a rather satisfactory agreement with the experiment at various engine operating conditions. Here it was assumed that good agreement is reached, if simulated and experimental data exhibit similar: injection timing, injection duration, fuelling, and maximal and mean injection pressure. Additionally, the pressure and needle lift histories should be roughly of the same shape. In this context, the agreement is overall very satisfactory and mainly within the error of experiment. Only the needle lift histories at low pump speeds exhibit a somewhat larger disagreement, which might be partially due to lower stability of the system at low speeds.

Based on these results, one may assume that the influence of different fuels on the injection characteristics at various operating regimes can be determined with reasonable accuracy by using the present simulation model. This model is capable of delivering results similar to the previously published model [6]. It should be noted, however, that the presented model has the important advantage of being relatively easily reproducible by any interested user. Even more, this kind of simulation setup makes possible to reduce the needed development time significantly. At the same time, the list of available output variables is typically quite extensive and the available output can be used to simulate spray formation [20], combustion process, and emissions [21,22], because the injection simulation module (AVL Boost™ Hydsim) can be connected to various other AVL software modules, such as AVL FIRE™, which is a CFD simulation tool in the field of combustion analysis that allows predicting with high accuracy all IC Engine relevant processes including injection nozzle flow, fuel injection, combustion,

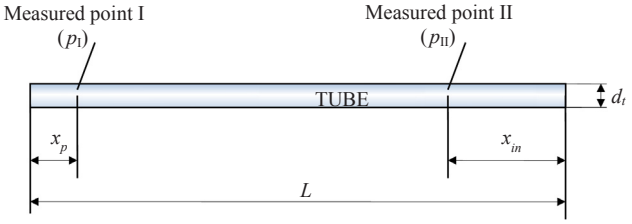

Fig. 5. Position of pressure sensors in the HP tube (x_p = 134.5 10^{-3} m and x_{in} = 35 10^{-3} m).

emission and exhaust gas after-treatment.

Finally, an example of an output parameter (mass injection rate history) obtained by simulation for a single operating regime and for all tested fuels is shown in Fig. 10. This output can be used as an input parameter for AVL FIRE™.

According to the obtained results, it might be worth commenting briefly on the usability of tested fuels in a diesel engine. Our previous investigations [14–16,7,17] show, that biodiesel fuel is a good alternative to mineral diesel and that bioethanol addition to biodiesel fuel (E15B85) brings B100 fuel properties close to those of mineral diesel. Consequently, the injection pressure history, injection duration, injection timing and mass injection rate (Figs. 6–10) are similar to those of mineral diesel. Therefore, it is reasonable to assume that the diesel engine characteristics (power, torque, fuel consumption …) obtained by E15B85 and D100 would be relatively close. In this view, the E15B85 fuel looks to be an attractive alternative fuel option for a diesel engine.

7. Conclusions

In the present study, a complete simulation model for an in-line injection system was developed. The mathematical model was built by using the AVL Boost™ Hydsim software, while the required input data were carefully derived by using the results of previous work, existing data, experimental measurements, and numerical simulation. The model was tested for accuracy and validated by comparing

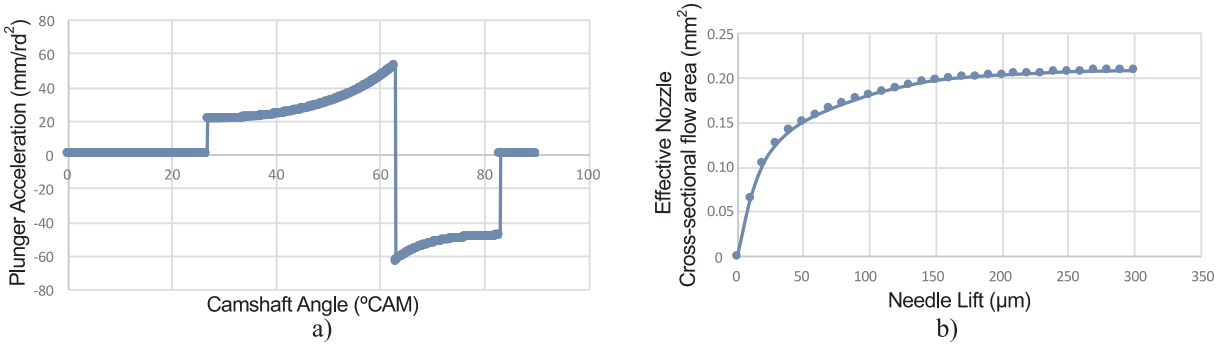

Fig. 4. a) Plunger acceleration, b) Effective nozzle cross-sectional flow area.

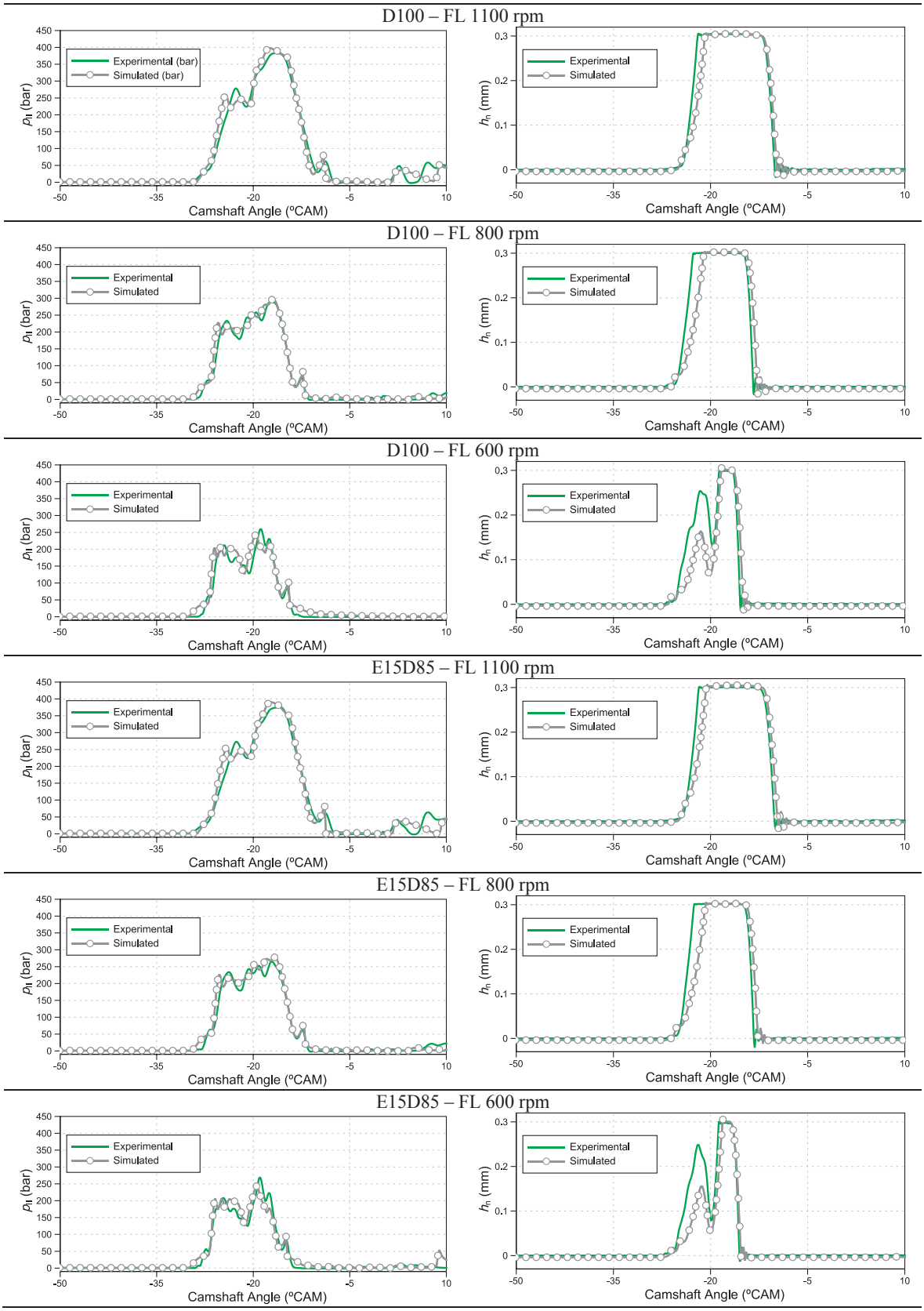

Fig. 6. Experimental and simulated needle lift h_n and injection pressure p_{II} for diesel fuel and bioethanol-diesel fuel blend at full load (FL) and several pump speeds, $T = 20$ °C.

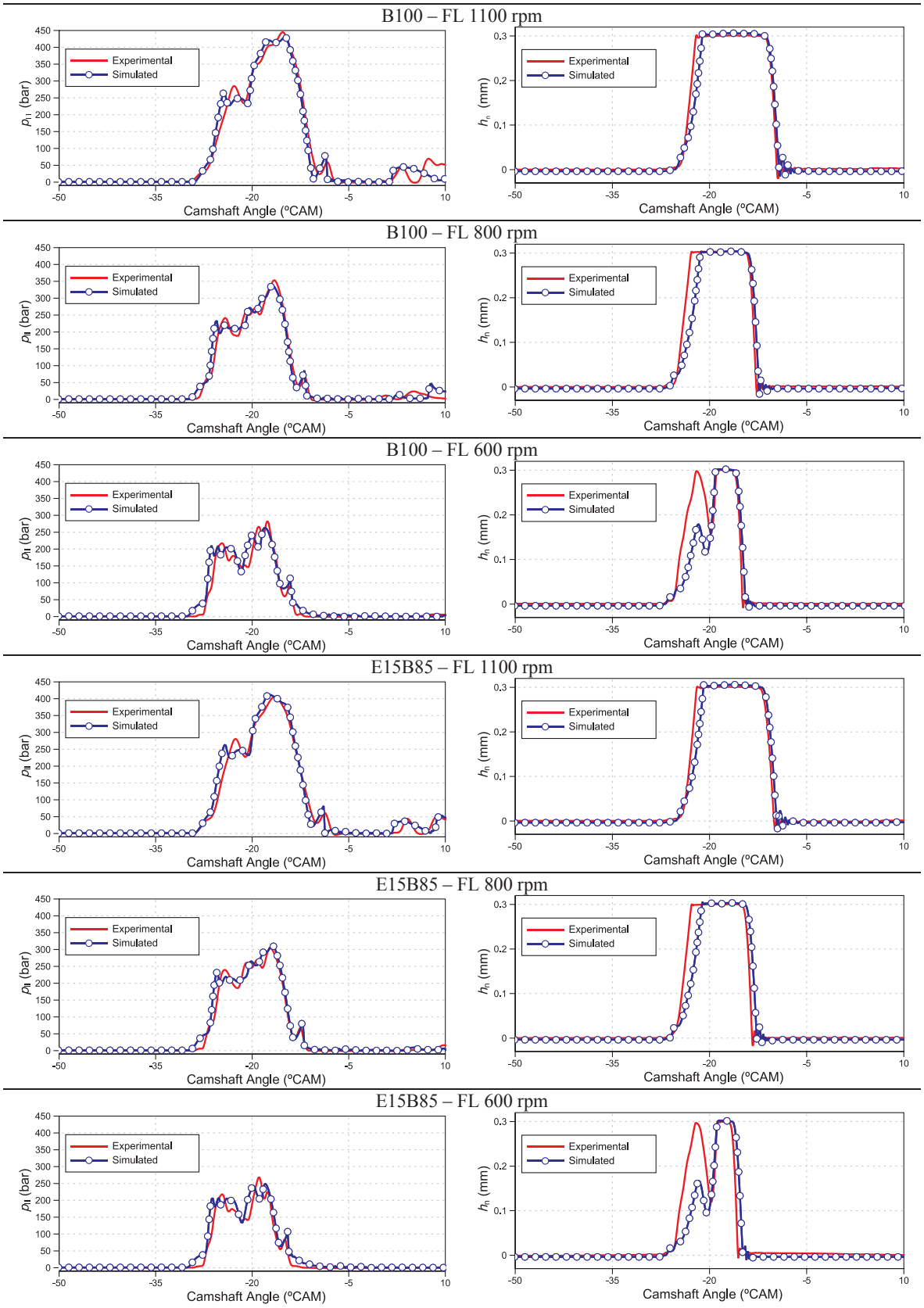

Fig. 7. Experimental and simulated needle lift h_n and pressure p_{II} for biodiesel and bioethanol-biodiesel fuel blend at full load (FL) and several pump speeds, $T = 20$ °C.

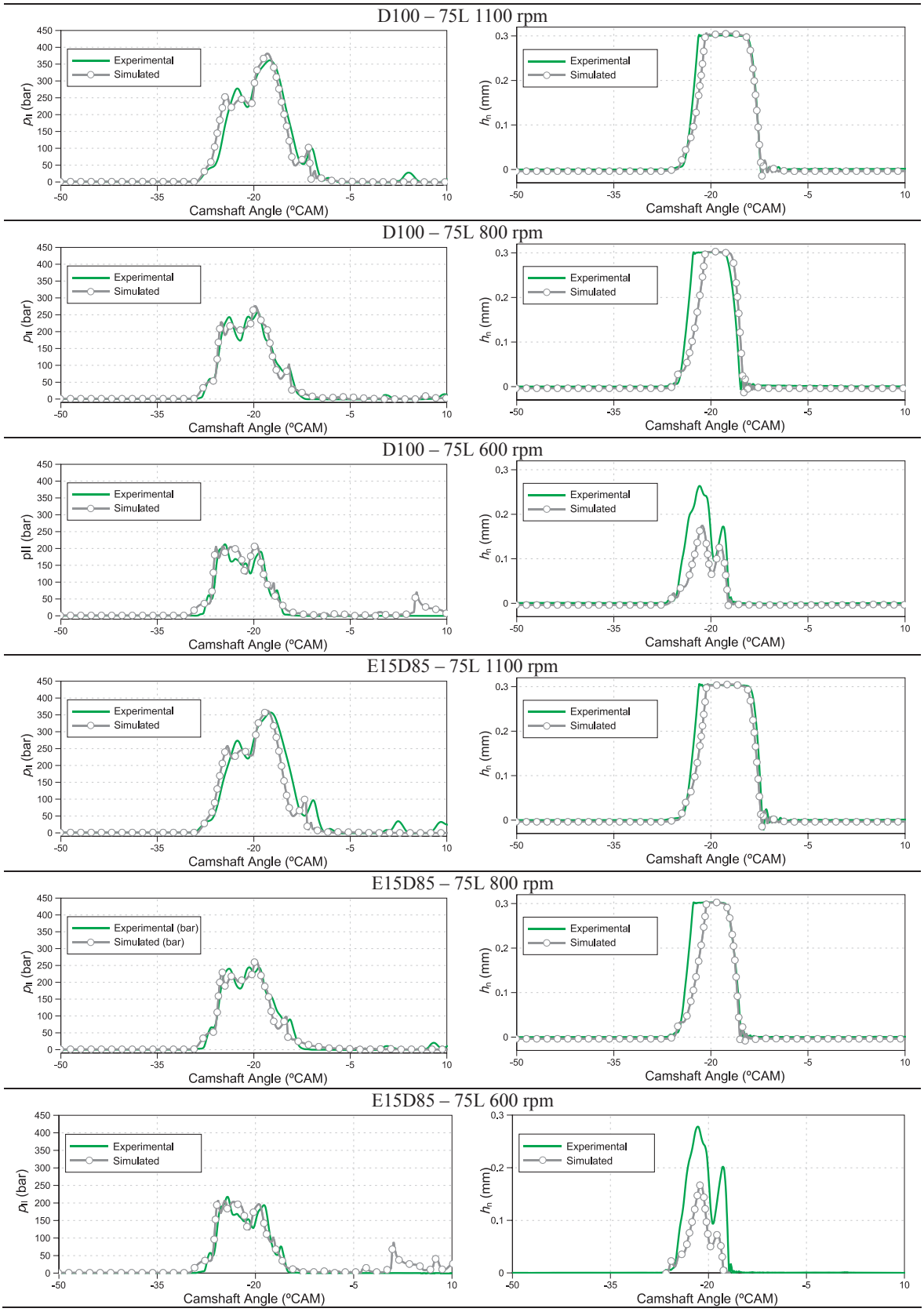

Fig. 8. Experimental and simulated needle lift h_n and injection pressure p_{II} for diesel and bioethanol-diesel fuel blend at 75% partial load (75L) and several pump speeds, $T = 20$ °C.

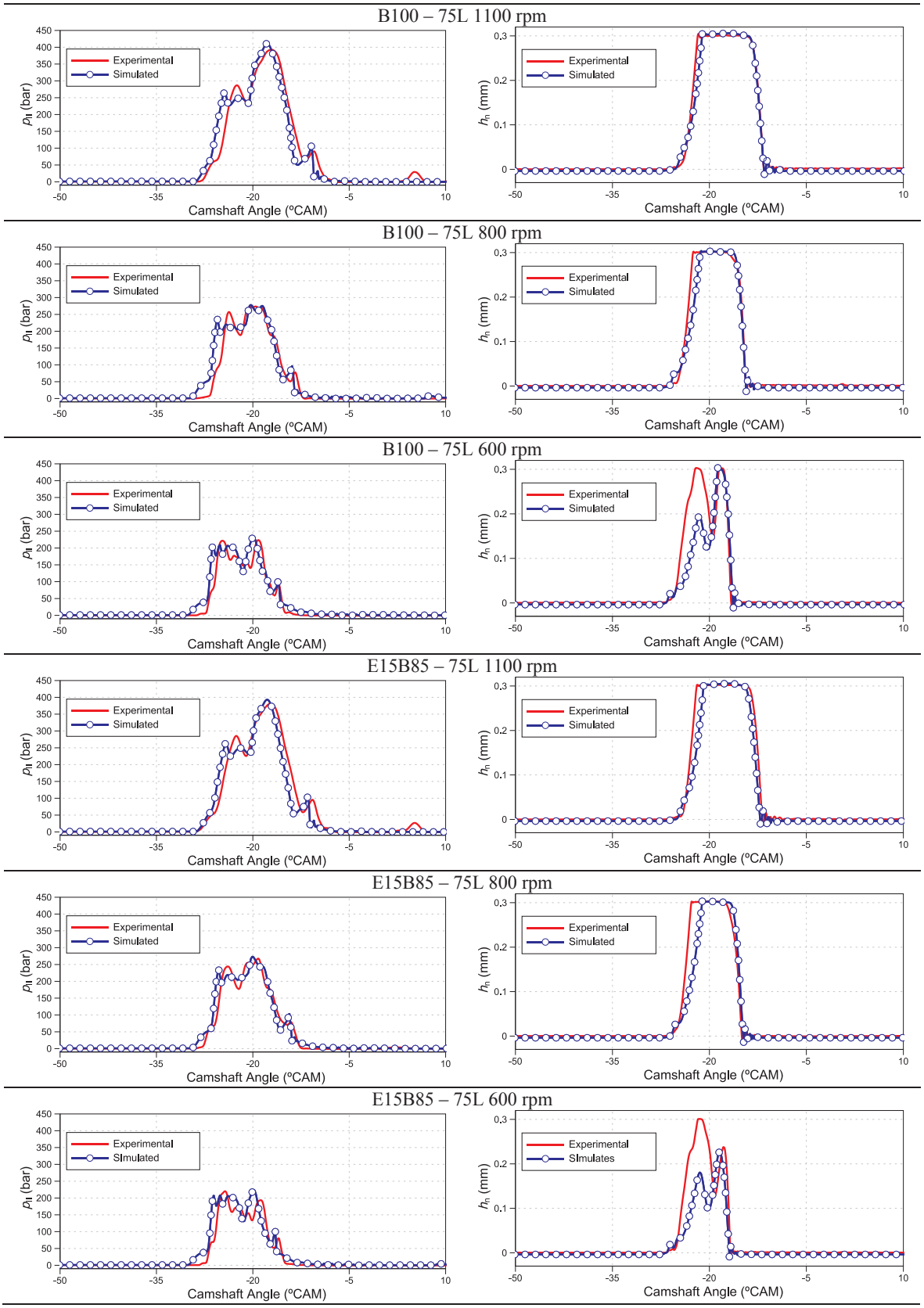

Fig. 9. Experimental and simulated needle lift h_n and injection pressure p_{II} for biodiesel and bioethanol-biodiesel fuel blend at 75% partial load (75L) and several pump speeds, $T = 20$ °C.

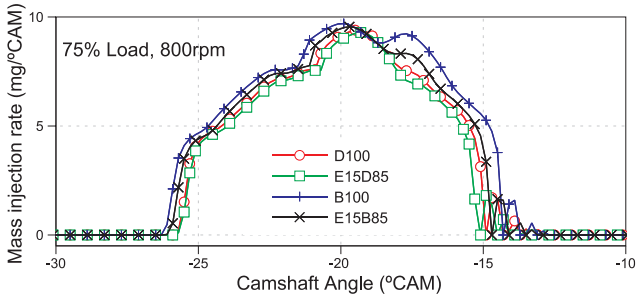

Fig. 10. Example of output parameters obtained from the simulation: mass injection rate.

experimental and numerically obtained injection pressure and needle lift histories. The comparison was done at full load and 75% partial load for various pump speeds (600, 800 and 1100 rpm) by considering a single injection assembly. According to the results, the following conclusions can be made:

1. The underlying mathematical model is capable to deliver satisfactory results at acceptable computational effort. It allows for simulation of many injection characteristics such as fuelling, injection timing, injection duration, mean injection rate, and maximum injection pressure. The model can be built or modified relatively easily and can be used also to produce input data needed for simulating subsequent processes, such as spray formation, combustion process, and the estimation of exhaust emissions.
2. Careful determination of model input data is of vital importance. Especially problematic are the properties of various biofuel blends, which are typically not known well enough. However, by making use of existing data, formulas and procedures described in this work, the presented model enables satisfactory simulations of injection processes at least for B100, D100, E15D85 and E15D85. Furthermore, the resulting model allows analysing the influence of bioethanol addition to biodiesel and diesel fuel on the injection process in view of harmful emission reduction.
3. According to the results, it might be also worth to comment on the performance of tested fuels. In general, one may say that adding bioethanol to biodiesel has a beneficial effect, because this brings biodiesel injection characteristics close to those of neat diesel. This might indicate an interesting potential to substitute diesel fuel in a renewable way without heavy engine modifications.

Acknowledgments

This research was supported by the Spanish Ministry of Economy and Competitiveness under research project ENE2014-57043-R. Authors are also grateful for the provision of Research Mobility Grants from “University of Jaén, Spain 2016” to E. Torres-Jimenez and to R. Dorado. The usage of the AVL Boost™ Hydsim software in the framework of the University Partnership Program of AVL List GmbH is greatly acknowledged.

References

[1] Koh H. Communicating the health effects of climate change. JAMA 2016;315:239–40.
[2] Manohar G, Devi SP, Rao KS. Evaluation of policies to reduce transportation pollution using system dynamics. Environ Prot Eng 2014;40:143–53.
[3] Arcoumanis C, Fairbrother RJ, Gavaises M, Flora H, French B. Development and validation of a computer simulation model for diesel fuel injection systems. Proc Inst Mech Eng Part D-J Automob Eng 1996;210:149–60.
[4] Kegl B An improved mathematical model of conventional FIE processes. SAE Technical Paper 950079 1995:17–25.
[5] Palomar JM, Cruz F, Ortega A, Jimenez-Espadafor FJ, Martinez G, Dorado MP. Development of a computer model to simulate the injection process of a diesel engine. Energy Fuels 2005;19:1526–35.
[6] Torres-Jimenez E, Kegl M, Dorado R, Kegl B. Numerical injection characteristics analysis of various renewable fuel blends. Fuel 2012;97:832–42.
[7] Kegl B. Numerical analysis of injection characteristics using biodiesel fuel. Fuel 2006;85:2377–87.
[8] https://www.avl.com/-/avl-boost-hydsim.
[9] Yamane K, Ueta A, Shimamoto Y. Influence of physical and chemical properties of biodiesel fuels on injection, combustion and exhaust emission characteristics in a direct injection compression ignition engine. Int J Engine Res 2001;2:249–61.
[10] Kegl B, Kegl M, Pehan S. Effects of biodiesel usage on injection process characteristics. In: Anonymous green diesel engines. Springer, 2013:127–52.
[11] Hansen AC, Zhang Q, Lyne PWL. Ethanol–diesel fuel blends—a review. Bioresour Technol 2005;96:277–85.
[12] Rakopoulos D, Rakopoulos C, Kakaras E, Giakoumis E. Effects of ethanol–diesel fuel blends on the performance and exhaust emissions of heavy duty DI diesel engine. Energy Convers Manage 2008;49:3155–62.
[13] Lapuerta M, Armas O, Herreros JM. Emissions from a diesel-bioethanol blend in an automotive diesel engine. Fuel 2008;87:25–31.
[14] Torres-Jimenez E, Svoljšak-Jerman M, Gregorc A, Lisec I, Dorado MP, Kegl B. Physical and chemical properties of ethanol diesel fuel blends. Fuel 2010;90:795–802.
[15] Torres-Jimenez E, Svoljšak-Jerman M, Gregorc A, Lisec I, Dorado MP, Kegl B. Physical and chemical properties of ethanol–biodiesel blends for diesel engines. Energy Fuels 2010;24:2002–9.
[16] Torres-Jimenez E, Pilar Dorado M, Kegl B. Experimental investigation on injection characteristics of bioethanol-diesel fuel and bioethanol-biodiesel blends. Fuel 2011;90:1968–79.
[17] Kegl B. Biodiesel usage at low temperature. Fuel 2008;87:1306–17.
[18] Watson G, Zéberg-Mikkelsen CK, Baylaucq A, Boned C. High-pressure density measurements for the binary system ethanol heptane. J Chem Eng Data 2006;51:112–8.
[19] Brennen CE. Cavitation and bubble dynamics. Cambridge University Press, 2013.
[20] Pogorevc P, Kegl B, Skerget L. Diesel and biodiesel fuel spray simulations. Energy Fuels 2008;22:1266–74.
[21] Lešnik L, Vajda B, Žunič Z, Škerget L, Kegl B. The influence of biodiesel fuel on injection characteristics, diesel engine performance, and emission formation. Appl Energy 2013;111:558–70.
[22] Lešnik L, Iljaž J, Hribernik A, Kegl B. Numerical and experimental study of combustion, performance and emission characteristics of a heavy-duty DI diesel engine running on diesel, biodiesel and their blends. Energy Convers Manage 2014;81:534–46.